Virtual Oscillator Control Subsumes Droop Control

Mohit Sinha, Florian Dörfler, Brian B. Johnson, and Sairaj V. Dhople

***Abstract*— In this paper we examine the amplitude and phase dynamics of power-electronic inverters in islanded microgrids that are controlled to emulate the dynamics of a class of weakly nonlinear Liénard-type oscillators. The general strategy of controlling inverters to emulate the behavior of Liénard-type oscillators is termed Virtual Oscillator Control (VOC), and it presents a compelling time-domain alternative to ubiquitous droop control methods which linearly trade off voltage frequencies and magnitudes with active and reactive power injections. In comparison to droop control, which assumes a priori that the network operates in a quasi-stationary sinusoidal steady state, VOC is a time-domain control strategy that globally stabilizes a desired sinusoidal steady state. The main, and somewhat surprising, result of this paper is that—when reduced to the sinusoidal steady state—the VOC dynamics correspond to those of droop control. Hence, VOC is a globally stabilizing control strategy that can deal with higher-order harmonics and includes droop control in the harmonic steady state. The results are intriguing, in that they suggest that droop control laws can be recovered from averaging the complex dynamics of a class of weakly nonlinear limit-cycle oscillators.**

I. Introduction

An islanded inverter-based microgrid is a collection of heterogeneous DC energy resources, e.g., photovoltaic (PV) arrays, fuel cells, and energy-storage devices, interfaced to an AC distribution network and operated independently from the bulk power system. Energy conversion is typically managed by power-electronics voltage source inverters. The vast majority of academic and industrial efforts adopt *droop control* [1]–[4] for real-time control of inverters. Drawing from the control of synchronous generators in bulk power systems, droop control linearly trades off the active and reactive power injection with the inverters' terminal-voltage amplitude and frequency.

As an alternative to droop control, we have recently proposed a communication-free decentralized control strategy wherein islanded inverters are regulated to mimic the dynamics of nonlinear deadzone-type limit-cycle oscillators [5]–[7]. This method is inspired by synchronization phenomena in complex networks of coupled oscillators, and is termed *Virtual Oscillator Control* (VOC). In general, VOC is executed by programming nonlinear differential equations of limit-cycle oscillators onto inverters' microcontrollers and utilizing pertinent sinusoidally varying oscillator dynamic states to construct the pulse-width modulation (PWM) control signal. It is worth emphasizing that VOC is a *time-domain* approach and stabilizes arbitrary initial conditions to a sinusoidal steady state; as such it is markedly different from droop control which operates on phasor quantities and presumes the existence of a quasi-stationary AC steady state; see Fig. 1. We refer also to [8], [9] for related time-domain control strategies in the same vein as VOC.

Extending our previous efforts in [5]–[7] where we have focused on a nonlinear deadzone oscillator to constitute the virtual oscillator, in this paper we investigate the voltage dynamics of power-electronic inverters controlled to emulate the dynamics of a general class of weakly nonlinear Liénard-type oscillators. Particular examples of Liénard oscillators include the deadzone oscillator and the ubiquitous Van der Pol oscillator. In general, Liénard-type oscillators are described by the second-order differential equation $\ddot{x}+f(x)\dot{x}+g(x)=0$, where $f(\cdot)$ (respectively $g(\cdot)$) are differentiable and even (respectively odd) functions [10], [11]. Under certain conditions on the functions $f(\cdot)$ and $g(\cdot)$, these dynamics admit a unique and almost globally asymptotically stable limit cycle (details are in Section III-A). Unless stated otherwise, in subsequent discussions where we reference VOC, we imply the control strategy is implemented with Liénard-type oscillators; also, inverters controlled with this approach are termed virtual-oscillator-controlled (VO-controlled) inverters.

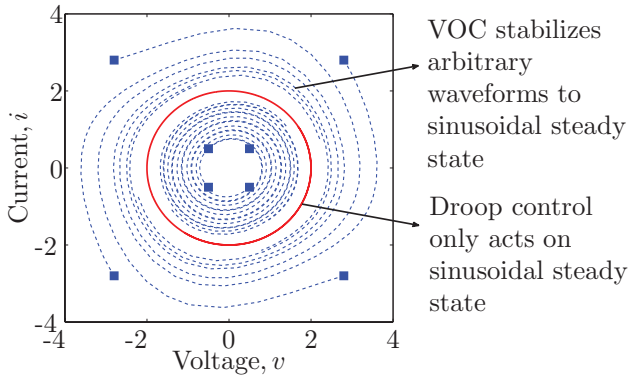

Fig. 1: VOC stabilizes arbitrary initial conditions to a sinusoidal steady state, while droop control acts on phasor quantities that are well defined only in the sinusoidal steady state. The main contribution of this work is to determine a set of parametric correspondences such that both control approaches admit identical dynamics in sinusoidal steady state.

M. Sinha and S. V. Dhople are with the Department of Electrical and Computer Engineering at the University of Minnesota (UMN), Minneapolis, MN (email: sinha052, sdhople@UMN.EDU). Their work was supported in part by the Institute of Renewable Energy and the Environment, UMN, under grant RL-0010-13; the Office of Naval Research under grant N000141410639; and the National Science Foundation under the CAREER award ECCS-1453921.

F. Dörfler is with the Automatic Control Laboratory at ETH Zürich, Zürich, Switzerland (email: dorfler@ETHZ.CH).

B. B. Johnson is with the Power Systems Engineering Center at the National Renewable Energy Laboratory (NREL), Golden, CO (email: brian.johnson@NREL.GOV). His work was supported by the Laboratory Directed Research and Development Program at NREL.

The main contribution of this paper relates to establishing a correspondence between VOC and droop control by obtaining conditions under which the respective voltage dynamics at the inverter terminals—close to the sinusoidal steady state—are identical. To bridge the temporal gap between droop control and VOC, the periodic Liénard-oscillator dynamics are averaged to focus on AC-cycle time scales [10], [12]. In addition to yielding insightful interpretations for droop control, our analysis highlights the choice of droop coefficients (equivalently, parameters of the Liénard-type oscillators) that would ensure droop-controlled inverters mimic the behavior of VO-controlled inverters close to the quasi-stationary sinusoidal steady state and vice versa (see Fig. 1). Furthermore, from a dynamical systems perspective, our analysis establishes connections between limit-cycle oscillators (VO-controlled inverters) and phase oscillators (droop-controlled inverters) which reaffirms similar connections and synchronization analyses for Van der Pol oscillators that date back to [13] and are recently surveyed in [14].

The remainder of this manuscript is organized as follows. Section II establishes notation and relevant mathematical preliminaries. In Section III, we introduce droop control and VOC. Next we derive time-averaged dynamics for weakly nonlinear Liénard type oscillators using tools from averaging theory in Section IV. Leveraging the averaged model, we establish a correspondence between droop control and VOC. We conclude the paper in Section V by highlighting a few pertinent directions for future work.

II. Notation and Preliminaries

The nominal system frequency is denoted by ω, and for the power-electronic inverters in the system, we assume that the instantaneous phase angle, ϕ, evolves according to

$$\frac{d\phi}{dt} = \omega + \frac{d\theta}{dt}, \tag{1}$$

where θ represents the phase offset with respect to the rotating reference frame established by ω. Denote the instantaneous current injected by the inverter as $i(t)$ and its instantaneous terminal voltage as $v(t)$. Since we are primarily interested in sinusoidal signals, we parameterize the instantaneous voltage as

$$v(t) := r(t)\cos(\omega t + \theta(t)), \tag{2}$$

where $r(t)$ is the instantaneous terminal-voltage amplitude. With this notation in place, we define the instantaneous active- and reactive-power injections as follows [15], [16]:

$$\begin{aligned} P(t) &:= v(t)i(t) = r(t)\cos(\omega t + \theta(t))i(t), \\ Q(t) &:= v(t-\pi/2)i(t) = r(t)\sin(\omega t + \theta(t))i(t). \end{aligned} \tag{3}$$

Assuming the fundamental frequency of the current injected by the inverter is ω, the average active and reactive power over an AC cycle (of period $2\pi/\omega$) are then given by

$$\overline{P} = \frac{\omega}{2\pi}\int_{\tau=0}^{2\pi/\omega} P(\tau)d\tau, \quad \overline{Q} = \frac{\omega}{2\pi}\int_{\tau=0}^{2\pi/\omega} Q(\tau)d\tau. \tag{4}$$

In subsequent developments, the time average of a periodic signal $u(t)$ with period T is denoted by $\overline{u}$, and defined as:

$$\overline{u} := \frac{1}{T}\int_0^T u(t)dt. \tag{5}$$

III. Fundamentals of VOC and Droop Control

In this section, we provide a brief introduction to droop control and VOC. We begin with an overview of Liénard systems, from which we recover a particular class of weakly nonlinear Liénard-type oscillators that the inverters are controlled to emulate.

A. Liénard systems

The celebrated Liénard's equation is a nonlinear second-order differential equation of the general form

$$\ddot{x} + f(x)\dot{x} + g(x) = 0. \tag{6}$$

This equation is commonly employed to study oscillations in nonlinear dynamical systems, e.g., the Van der Pol oscillator dynamics can be recovered as a special case of Liénard's equation [11]. The following theorem establishes conditions that the functions $f(\cdot)$ and $g(\cdot)$ have to satisfy such that the system (6) exhibits a unique and stable limit cycle.

Theorem 1 (Liénard's Theorem [17]). *Consider the second-order nonlinear dynamical system* (6)*. Assume that the functions $f(x)$ and $g(x)$ satisfy the following properties:*

(A1) $f(x)$ and $g(x)$ are continuously differentiable $\forall x$;

(A2) $g(x) > 0, \forall x > 0$; and $g(x)$ is an odd function, i.e., $g(-x) = -g(x), \forall x$;

(A3) $f(x)$ is an even function, i.e., $f(-x) = f(x), \forall x$;

(A4) The odd function $F(x) := \int_0^x f(\tau)d\tau$ has exactly one positive zero at $x = z$, is negative for $0 < x < z$, is positive and nondecreasing for $x > z$, and $F(x) \to \infty$ as $x \to \infty$.

Then, the system (6) *has a unique and stable limit cycle surrounding the origin in the phase plane.*

We next utilize the observations in Theorem 1 to synthesize a class of weakly nonlinear Liénard oscillators that the inverters are controlled to emulate. In particular, we focus on a parametric regime under which the trajectories of VO-controlled inverters approximate circular limit cycles to guarantee high power quality, i.e., the waveforms are almost sinusoidal with arbitrarily small higher-order harmonics. Furthermore, it is under this regime that we are able to establish correspondences with droop control.

B. VOC implemented with a class of Liénard-type oscillators

The implementation of VOC is accomplished with a class of weakly nonlinear and externally forced Liénard-type oscillators with dynamics of the general form

$$\ddot{x} + \varepsilon f(x)\dot{x} + \omega^2 x = \varepsilon\omega\dot{u}(t), \tag{7}$$

where $f : \mathbb{R} \to \mathbb{R}$ satisfies the conditions in Theorem 1, ω and ε are positive real constants, and $u(t)$ is a driving input by virtue of coupling the oscillator to the network.

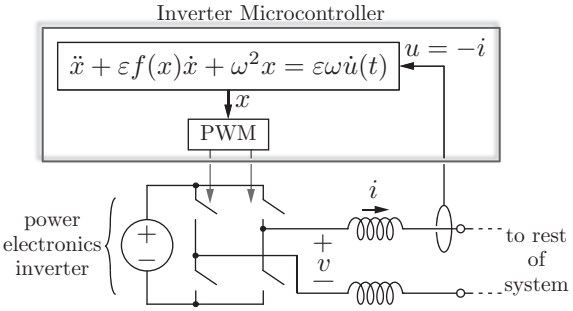

Fig. 2: Implementation of VOC for a single-phase power-electronic inverter. The inverter terminal current, i, is the driving term for the Liénard system, and the state x is utilized as the PWM modulation signal.

For an unforced oscillator, nearly sinusoidal oscillations with frequency approximately equal to ω are recovered in the so-called *quasi-harmonic regime* characterized by $\varepsilon \searrow 0$ [10], [11]. A detailed discussion on the properties of forced Liénard systems can be found in [18].

Remark. The implementation of the proposed controller is depicted in Fig. 2. In particular, notice that the state variable x takes the connotation of a voltage that the inverter terminals are controlled to emulate (this is accomplished through a pulse-width modulation block, see, e.g., [19] for more details). Furthermore, the input u corresponds to the current that is injected into the inverter output terminals. To respect circuit laws, the forcing term in the Liénard oscillator is therefore picked to be $\dot{u}$. (See also Fig. 3 and Corollary 1, where we discuss the Van der Pol oscillator circuit, a particular type of Liénard oscillator.)

C. Droop control

For resistive networks, droop control linearly trades off frequency deviation versus reactive-power injection; and inverter terminal-voltage amplitude versus active-power injection as follows [2], [20]:

$$\begin{aligned} \dot{\bar{\theta}} &= n\left(\overline{Q} - \overline{Q}^*\right), \\ \bar{r} - \bar{r}^* &= m\left(\overline{P}^* - \overline{P}\right). \end{aligned} \tag{8}$$

Here $\overline{Q}^*$ and $\overline{P}^*$ are the per-phase average reactive-power and active-power setpoints, respectively; $\bar{r}^*$ is the terminal-voltage-amplitude setpoint; and $n, m > 0$ are reactive-power and active-power droop coefficients, respectively. As expressed in (8), we assume that the droop laws are executed with AC-cycle averages of active and reactive power for each inverter.

IV. Uncovering Droop laws in Averaged VOC Dynamics

To bridge the time-scale separation between VOC (that is implemented in real-time) and droop control (that presumes the existence of a quasi-stationary sinusoidal steady state), we average the dynamics of the Liénard-type oscillator in (7). This averaging analysis allows us to focus on AC-cycle time scales and facilitates the derivation of correspondences with the droop laws in (8). To this end, we first uncover the voltage-amplitude and phase dynamics of VO-controlled inverters by transitioning to polar coordinates.

A. Polar-coordinates representation of Liénard-type oscillator dynamics

We begin by establishing a state-space model in Cartesian coordinates; in this regard we choose $y := \omega \int_0^t x dt$, and $z := x$ as states and write (7) as:

$$\dot{y} = \omega z, \quad \dot{z} = -\omega y + \varepsilon g(z) + \varepsilon\omega u(t), \tag{9}$$

where (with a slight abuse of notation with regard to (6)) we denote $g(z) := -\int f(z)dz$ in all subsequent developments. Consider the following bijective transformation of the states of the Liénard-type oscillator (7) to polar coordinates $[r, \theta]^{\mathrm{T}}$ in a rotating frame at frequency ω:

$$y = r\sin(\omega t + \theta), \quad z = r\cos(\omega t + \theta). \tag{10}$$

This bijective change of coordinates is well-defined (and leads to smooth dynamics) whenever $r \neq 0$ or equivalently $[y, z]^{\mathrm{T}} \neq 0$. Since the origin $[y, z]^{\mathrm{T}} = 0$ is unstable for the Liénard dynamics (7) [10] and not of interest to our application in AC microgrid networks, we assume in the following that $[y(0), z(0)]^{\mathrm{T}} \neq 0$ and thus $[y(t), z(t)]^{\mathrm{T}} \neq 0$ for all $t \geq 0$.

With the dynamical model (in polar coordinates) in place, we will leverage notions of averaging to focus on AC-cycle time scales. Given a time-varying dynamical system $\dot{x} = \varepsilon f(x, t, \varepsilon)$ with time-periodic vector field $f(x, t, \varepsilon) = f(x, t + T, \varepsilon)$ with period $T > 0$ and a small parameter $\varepsilon > 0$, we denote by $\dot{\bar{x}} = \varepsilon f_{\text{avg}}(\bar{x})$ the associated *time-averaged dynamical system* with vector field $f_{\text{avg}}(\bar{x}) = (1/T)\int_0^T f(\bar{x}, \tau, 0)d\tau$. The following result is an adaptation of the analysis of weakly nonlinear oscillators in [10, Chapter 10.5] and [12].

Lemma 1. *Consider the class of weakly nonlinear Liénard-type oscillators with dynamics in Cartesian coordinates expressed as in* (7)*. Let* $[r,\ \theta]^{\mathrm{T}} \in \mathbb{R}_{>0} \times \mathbb{S}$ *(*$\mathbb{S}$ *is the unit circle) denote the corresponding dynamics in polar coordinates in a rotating reference frame established by* ω*. Then, the time-averaged dynamics in polar coordinates in the quasi-harmonic limit,* $\varepsilon \searrow 0$*, are given by*

$$\begin{bmatrix} \dot{\bar{r}} \\ \dot{\bar{\theta}} \end{bmatrix} = \frac{\varepsilon}{2\pi} \begin{bmatrix} -\overline{f}(\bar{r}) + \omega^2 \int_0^{\frac{2\pi}{\omega}} u(t)\cos(\omega t + \bar{\theta})dt \\ -\omega^2 \int_0^{\frac{2\pi}{\omega}} \frac{u(t)}{\bar{r}}\sin(\omega t + \bar{\theta})dt \end{bmatrix}, \tag{11}$$

where

$$\overline{f}(\bar{r}) := 4\int_0^{\bar{r}} f(\sigma)\sqrt{1 - \frac{\sigma^2}{\bar{r}^2}}\, d\sigma. \tag{12}$$

Proof. To study the dynamics in the quasi-harmonic limit, i.e., $\varepsilon \searrow 0$, we begin by rewriting the dynamics (9) in polar coordinates. The dynamics in this new set of coordinates can then be simplified by leveraging tools from averaging theory [10, Theorem 10.4].

1) Change of coordinates: We begin by transforming (9) to polar coordinates (10) resulting in the following dynamics:

$$\dot{r} = \varepsilon\Big(g(r\cos(\omega t+\theta)) + \omega u(t)\Big)\cos(\omega t+\theta),$$
$$\dot{\theta} = -\frac{\varepsilon}{r}\Big(g(r\cos(\omega t+\theta)) + \omega u(t)\Big)\sin(\omega t+\theta). \quad (13)$$

2) Averaging: Note that the dynamical systems in (13) are $2\pi/\omega$-periodic functions in t. Using ε as the *small parameter*, we obtain the averaged dynamics

$$\begin{bmatrix}\dot{\overline{r}}\\ \dot{\overline{\theta}}\end{bmatrix} = \frac{\varepsilon\omega}{2\pi}\int_0^{2\pi/\omega}\begin{bmatrix} g(\overline{r}\cos(\omega t+\overline{\theta}))\cos(\omega t+\overline{\theta})\\ -\frac{1}{\overline{r}}g(\overline{r}\cos(\omega t+\overline{\theta}))\sin(\omega t+\overline{\theta})\end{bmatrix}dt + \frac{\varepsilon\omega^2}{2\pi}\int_0^{2\pi/\omega}\begin{bmatrix} u(t)\cos(\omega t+\overline{\theta})\\ -\frac{1}{\overline{r}}u(t)\sin(\omega t+\overline{\theta})\end{bmatrix}dt. \quad (14)$$

We introduce a change of variable on the right hand side, $\overline{\phi} = \omega t + \overline{\theta}$ to obtain:

$$\begin{bmatrix}\dot{\overline{r}}\\ \dot{\overline{\theta}}\end{bmatrix} = \frac{\varepsilon}{2\pi}\int_0^{2\pi}\begin{bmatrix} g(\overline{r}\cos\overline{\phi})\cos\overline{\phi}\\ -\frac{1}{\overline{r}}g(\overline{r}\cos\overline{\phi})\sin\overline{\phi}\end{bmatrix}d\overline{\phi} + \frac{\varepsilon\omega}{2\pi}\int_0^{2\pi}\begin{bmatrix} u(t)\cos\overline{\phi}\\ -\frac{1}{\overline{r}}u(t)\sin\overline{\phi}\end{bmatrix}d\overline{\phi}. \quad (15)$$

Since $g(\overline{r}\cos\overline{\phi})$ is an even function in $\overline{\phi}$, it follows that $g(\overline{r}\cos\overline{\phi})\sin\overline{\phi}$ is an odd function in $\overline{\phi}$, and $g(\overline{r}\cos\overline{\phi})\cos\overline{\phi}$ is an even function in $\overline{\phi}$. Using these observations, for the integral in (15) involving $g(\overline{r}\cos\overline{\phi})\sin\overline{\phi}$, we get:

$$\int_0^{2\pi} g(\overline{r}\cos\overline{\phi})\sin\overline{\phi}\,d\phi = 0. \quad (16)$$

Similarly, for the integral in (15) involving $g(\overline{r}\cos\overline{\phi})\cos\overline{\phi}$, we get

$$\begin{aligned}&\int_0^{2\pi} g(\overline{r}\cos\overline{\phi})\cos\overline{\phi}d\overline{\phi}\\ &= 4\int_0^{\pi/2} g(\overline{r}\cos\overline{\phi})\cos\overline{\phi}d\overline{\phi}\\ &= 4g(\overline{r}\cos\overline{\phi})\sin\overline{\phi}\big|_0^{\pi/2} + 4\int_0^{\pi/2} f(\overline{r}\cos\overline{\phi})\overline{r}\sin^2\overline{\phi}d\overline{\phi}\\ &= -4\int_0^{\overline{r}} f(\sigma)\sqrt{1-\frac{\sigma^2}{\overline{r}^2}}d\sigma = -\overline{f}(\overline{r}),\end{aligned} \quad (17)$$

where the last line in (17) follows from applying the change of variables $\sigma = \overline{r}\cos\overline{\phi}$ [12]. Applying the change of time coordinates, $\overline{\phi} = \omega t + \overline{\theta}$, and leveraging the observations in (16) and (17), we see that the averaged dynamics in polar coordinates of the Liénard-type oscillators in (7) admit the representation in (11). □

B. Uncovering droop laws in Liénard oscillator dynamics

In this section, we derive the conditions under which the droop control laws (8) closely match those of VO-controlled inverters with dynamics represented by Liénard's equation (7). To establish the connection between the virtual oscillator and the physical inverter, we assume that the inverter terminal voltage is controlled to follow the signal $r(t)\cos(\omega t+\theta)$ (2); similarly, to close the loop, the inverter output current $i(t)$ is extracted from the virtual oscillator, i.e., $u(t) = -i(t)$. This allows us to make the connection between the polar-coordinate system-dynamics representation in (13) and the notions of average active and reactive power in (4). In particular, from (11), we see that the averaged voltage amplitude dynamics can be written as

$$\begin{aligned}\dot{\overline{r}} &= \varepsilon\Big(-\frac{1}{2\pi}\overline{f}(\overline{r}) + \frac{\omega^2}{2\pi}\int_0^{\frac{2\pi}{\omega}}\frac{-i(t)}{\overline{r}}\overline{r}\cos(\omega t+\overline{\theta})dt\Big),\\ &= -\frac{\varepsilon}{2\pi}\overline{f}(\overline{r}) - \varepsilon\omega\frac{\overline{P}}{\overline{r}},\end{aligned} \quad (18)$$

where we have used the definition of average active power, $\overline{P}$, from (4). Similarly, the averaged voltage phase dynamics can be written as

$$\dot{\overline{\theta}} = -\frac{\varepsilon\omega^2}{2\pi}\int_0^{\frac{2\pi}{\omega}}\frac{-i(t)}{\overline{r}^2}\overline{r}\sin(\omega t+\overline{\theta})dt = \frac{\varepsilon\omega}{\overline{r}^2}\overline{Q}, \quad (19)$$

where we have used the definition of average reactive power, $\overline{Q}$, from (4). Therefore, the averaged VOC dynamics in the quasi-harmonic limit, $\varepsilon \searrow 0$, can be written as:

$$\dot{\overline{r}} = \left(-\frac{2\varepsilon}{\pi}\int_0^{\overline{r}} f(\sigma)\sqrt{1-\frac{\sigma^2}{\overline{r}^2}}d\sigma\right) - \varepsilon\omega\frac{\overline{P}}{\overline{r}}, \quad (20a)$$
$$\dot{\overline{\theta}} = +\frac{\varepsilon\omega}{\overline{r}^2}\overline{Q}. \quad (20b)$$

In the following, we analyze how the droop laws and coefficients should be designed so that the difference in the phase dynamics and steady-state equilibrium voltage profile of the two inverters (controlled with VOC and droop) is of order $\mathcal{O}(\varepsilon)$. When comparing the droop control law (8) with the averaged VOC dynamics (20) (reduced to the limit cycle), we arrive at the following correspondence:

Theorem 2 (Correspondence between Droop Control and VOC). *Consider two identical inverters one of which is controlled with VOC* (13)*, and the other is controlled with droop control* (8)*. Let $\bar{r}$ and $\bar{\theta}(t)$ denote the amplitudes and phases as used in droop control, and $r(t)$ and $\theta(t)$ are the amplitudes and phases in VOC. Assume that*

(A1) unique solutions to the droop-controlled system (8) *and the averaged VOC system* (20) *exist in a time interval $t \in [0, t^*]$ of strictly positive length; and*

(A2) the initial signal differences (at time $t = 0$) are of order $\mathcal{O}(\varepsilon)$, that is,

$$\bar{r} - r(0) \approx \mathcal{O}(\varepsilon) \quad \text{and} \quad \bar{\theta}(0) - \theta(0) \approx \mathcal{O}(\varepsilon).$$

Denote the equilibrium terminal-voltage amplitude and average active-power injection of the VO-controlled inverter by $\overline{r}_{\rm eq}$ and $\overline{P}_{\rm eq}$, respectively. Suppose the frequency-droop coefficient is picked as

$$n = \frac{\varepsilon\omega}{\overline{r}_{\rm eq}^2}, \quad (21)$$

and the average reactive-power setpoint is set to zero, $\overline{Q}^* = 0$. Suppose the voltage-droop coefficient is picked as

$$m = \left(\frac{2\overline{r}_{\rm eq}}{\omega\pi} \int_0^{\overline{r}_{\rm eq}} \frac{f(\sigma)}{\sqrt{\overline{r}_{\rm eq}^2 - \sigma^2}} d\sigma \right)^{-1}, \qquad (22)$$

and the average active-power and amplitude setpoints are set as $\overline{P}^* = \overline{P}_{\rm eq}$ and $\overline{r}^* = \overline{r}_{\rm eq}$. Then, there exists an ε^*, such that for all $0 < \varepsilon < \varepsilon^*$, for all $t \in [0, t^*]$

$$\bar{r} - r(t) \approx \mathcal{O}(\varepsilon) \quad \text{and} \quad \bar{\theta}(t) - \theta(t) \approx \mathcal{O}(\varepsilon).$$

Since the droop coefficients themselves depend on $\overline{r}_{\rm eq}$ and $\overline{P}_{\rm eq}$ in the quasi-harmonic limit $\varepsilon \searrow 0$, close to the quasi-stationary sinusoidal steady state, VOC can be thought of as an adaptive droop controller with load-dependent droop coefficients. The correspondences derived in Theorem 2 are asymptotic results based on a perturbation and averaging analysis for sufficiently small ε.

Proof of Theorem 2. Under the given assumptions (A1) and (A2), by standard averaging arguments [10, Theorem 10.4], there exists an ε_1^* sufficiently small so that for all $0 < \varepsilon < \varepsilon_1^*$, the solution of the averaged VOC dynamics (20) is $\mathcal{O}(\varepsilon)$ close to the solution of the original VOC dynamics (7) for times $t \in [0, t^*/\varepsilon]$. We proceed by comparing the averaged VOC system (20) with the droop control system (8).

1) Correspondence of phase dynamics: We first study the phase dynamics (20b). The VOC system (7) is assumed to evolve in quasi-stationary sinusoidal steady state with a small initial (at time $t = 0$) difference from the harmonic droop signals. Recall that in the quasi-harmonic limit, there exists an ε_2^* sufficiently small so that for all $0 < \varepsilon < \varepsilon_2^*$, the solution of the VOC dynamics (7) is $\mathcal{O}(\varepsilon)$ close to the solution of the harmonic oscillator with constant radius $\overline{r}_{\rm eq}$ for $t \in [0, t^*]$; see [10, Theorem 10.1 and Example 10.3]. Hence, for $t \in [0, t^*]$, the solution $\overline{\theta}(t)$ of the averaged phase dynamics (20b) is $\mathcal{O}(\varepsilon)$ close to the solution of

$$\dot{\overline{\theta}} = \frac{\varepsilon\omega}{\overline{r}_{\rm eq}^2} \overline{Q},$$

where we disregard the amplitude dynamics (20a), and replace $\overline{r}(t)$ in (20b) by $\overline{r}_{\rm eq}$.

For the following arguments, let $0 \leq \varepsilon \leq \min\{\varepsilon_1^*, \varepsilon_2^*\}$. Observe that the phase dynamics of a droop-controlled inverter (8) correspond with the AC-cycle-averaged dynamics of a VO-controlled inverter (7)—up to an order $\mathcal{O}(\varepsilon)$ mismatch—if we pick the reactive-power setpoint, $\overline{Q}^*$, and the frequency-droop coefficient, n, as follows:

$$\overline{Q}^* = 0, \quad n = \frac{\varepsilon\omega}{\overline{r}_{\rm eq}^2}. \qquad (23)$$

2) Correspondence of equilibrium voltage amplitudes: Next, we consider the amplitude dynamics (20a) and its equilibrium terminal-voltage profile. The steady-state voltage amplitude of the VO-controlled inverter is recovered from the solution of the following nonlinear equation:

$$0 = \left(-\frac{2\varepsilon}{\pi} \int_0^{\overline{r}} f(\sigma) \sqrt{1 - \frac{\sigma^2}{\overline{r}^2}} d\sigma \right) - \varepsilon\omega \frac{\overline{P}}{\overline{r}} \qquad (24)$$

Around the solution of (24), which we denote by $\overline{r}_{\rm eq}$, we obtain the sensitivity of the active-power injection with respect to a change in amplitude:

$$\left. \frac{d\overline{P}_{\rm eq}}{d\overline{r}_{\rm eq}} \right|_{\overline{r}_{\rm eq}} = -\frac{2\overline{r}_{\rm eq}}{\omega\pi} \int_0^{\overline{r}_{\rm eq}} \frac{f(\sigma)}{\sqrt{\overline{r}_{\rm eq}^2 - \sigma^2}} d\sigma. \qquad (25)$$

The equation (25) can be placed in correspondence with the amplitude control law of a droop-controlled inverter (8). By an analogous reasoning as for the phase dynamics, there exists an ε_3^* sufficiently small so that for all $0 < \varepsilon < \varepsilon_3^*$, the solution $\overline{r}(t)$ of the averaged amplitude dynamics (20a) satisfies—up to an $\mathcal{O}(\varepsilon)$ mismatch—the conditions of the stationary solution (25) (with fixed radius $\overline{r}_{\rm eq}$) for strictly positive times $t \in [0, t^*]$. For the following arguments, let $0 \leq \varepsilon \leq \min\{\varepsilon_1^*, \varepsilon_3^*\}$. Observe that the amplitude dynamics of a droop-controlled inverter (8) correspond with that of a VO-controlled inverter in (25)—up to an order $\mathcal{O}(\varepsilon)$ mismatch—if we pick the active-power setpoint, $\overline{P}^*$, terminal-voltage setpoint, $\overline{r}^*$, and the voltage-droop coefficient, m, as follows:

$$\overline{P}^* = \overline{P}_{\rm eq}, \ \overline{r}^* = \overline{r}_{\rm eq},$$
$$m = \left(\frac{2\overline{r}_{\rm eq}}{\omega\pi} \int_0^{\overline{r}_{\rm eq}} \frac{f(\sigma)}{\sqrt{\overline{r}_{\rm eq}^2 - \sigma^2}} d\sigma \right)^{-1}. \qquad (26)$$

Finally, to complete the proof let $\varepsilon^* = \min\{\varepsilon_1^*, \varepsilon_2^*, \varepsilon_3^*\}$, and note that all arguments hold for the time scales $[0, t^*/\varepsilon^*] \cap [0, t^*]$ which equals $[0, t^*]$ for ε^* sufficiently small. □

C. The Van der Pol oscillator

Consider the ubiquitous Van der Pol oscillator to constitute the virtual oscillator circuit for inverter control. The equivalent circuit of this oscillator is composed of an RLC circuit connected in parallel to a nonlinear voltage-dependent current source (see Fig. 3). The dynamics of the oscillator are captured by the following second-order nonlinear ODE:

$$\ddot{x} - \varepsilon\omega\alpha \left(1 - \beta x^2\right) \dot{x} + \omega^2 x = \varepsilon\omega \dot{u}(t), \qquad (27)$$

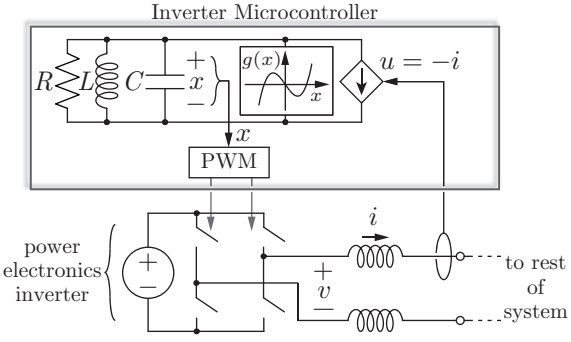

Fig. 3: Implementation of VOC for a single-phase power-electronic inverter with a Van der Pol oscillator. The oscillator is composed of a parallel RLC circuit, and a nonlinear voltage-dependent current source, $g(x)$. The inverter terminal current, i, is the driving term, and the sinusoidal capacitor voltage, x, is utilized as the PWM modulation signal.

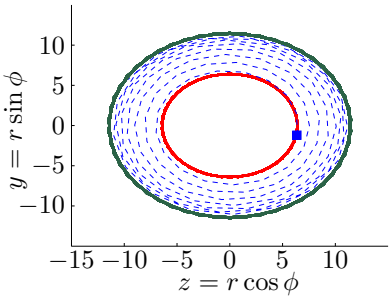

Fig. 4: (Red limit cycle): Droop control before load step; (Green limit cycle): Droop control post load step; (Dashed-blue line): Evolution of VOC starting from the initial condition illustrated as a blue square. Simulation parameters: $\varepsilon = 0.09$, $\sigma = 1\text{S}$, $R = 10\Omega$, $L = 250\mu\text{H}$, $C = 30.9\text{mF}$. Load step: $0.2\Omega \to 500\Omega$.

where x is the voltage that develops across the capacitor C, and we have the following parameters: $\varepsilon := \sqrt{L/C}$, $\alpha := \sigma - (1/R)$, and $\beta := 3k/(\sigma - \frac{1}{R})$ for some $k > 0$. With reference to the model in (7), we see that $f(x) = (\beta x^2 - 1)\alpha\omega$, and subsequently, $g(x) = -\int f(x)dx = \alpha\omega(x - \beta x^3/3)$. Notice that $g(x)$ is the nonlinear voltage-dependent current source in the circuit representation. Furthermore, for $\varepsilon \searrow 0$ and no input, $u = 0$, the Van der Pol oscillator exhibits near sinusoidal oscillations with frequency $\omega = 1/\sqrt{LC}$. For an islanded inverter controlled as a Van der Pol oscillator, we have the following corollary to Theorem 2.

Corollary 1 (VOC with Van der Pol oscillator). *The droop coefficients that would ensure droop-controlled inverters mimic the behavior of Van der Pol oscillator-controlled inverters close to the quasi-stationary sinusoidal steady state are given by:*

$$n = \frac{1}{\overline{r}_{\text{eq}}^2 C}, \quad m = -\frac{1}{\alpha\left(\overline{r}_{\text{eq}} - \frac{\beta}{2}\overline{r}_{\text{eq}}^3\right)}. \tag{28}$$

Proof. The result follows from substituting $\varepsilon = \sqrt{L/C}$, $\omega = 1/\sqrt{LC}$, and $f(x) = (\beta x^2 - 1)\alpha\omega$ in (21) and (22). □

Numerical Simulation. Consider two inverters serving a resistive load; one controlled with droop control and the other controlled to emulate the Van der Pol oscillator dynamics in (27). The droop coefficients are picked based on (28). Trajectories from a numerical simulation are plotted in polar coordinates in Fig. 4. The red and green limit cycles are obtained for the droop-controlled inverter before and after a load step. The trajectory in blue (starting from an initial condition illustrated as a blue square) results from the dynamics in (27). The simulations indicate that with the droop control parameters chosen based on (28), the dynamics of VOC correspond to that of droop control when reduced to the sinusoidal steady state.

V. Conclusions

For a system of power-electronic inverters controlled as a class of weakly nonlinear Liénard-type oscillators, we characterized the voltage dynamics in polar coordinates to establish a set of conditions for which the dynamics of the Liénard-type oscillators match the classical droop laws. Leveraging the obtained averaged dynamics to design control strategies for general microgrid networks remain the focus of ongoing investigations.

Acknowledgments

F. Dörfler would like to thank Rodolphe Sepulchre and Pierre Sacré for insightful discussions.

References

[1] M. C. Chandorkar, D. M. Divan, and R. Adapa, "Control of parallel connected inverters in standalone AC supply systems," *IEEE Transactions on Industry Applications*, vol. 29, pp. 136–143, January 1993.
[2] Q.-C. Zhong, "Robust droop controller for accurate proportional load sharing among inverters operated in parallel," *IEEE Transactions on Industrial Electronics*, vol. 60, no. 4, pp. 1281–1290, 2013.
[3] N. Pogaku, M. Prodanovic, and T. Green, "Modeling, analysis and testing of autonomous operation of an inverter-based microgrid," *IEEE Transactions on Power Electronics*, vol. 22, pp. 613–625, March 2007.
[4] A. Bidram and A. Davoudi, "Hierarchical structure of microgrids control system," *IEEE Transactions on Smart Grid*, vol. 3, no. 4, pp. 1963–1976, 2012.
[5] B. B. Johnson, S. V. Dhople, A. O. Hamadeh, and P. T. Krein, "Synchronization of Nonlinear Oscillators in an LTI Electrical Power Network," *IEEE Transactions on Circuits and Systems I: Regular Papers*, vol. 61, pp. 834–844, March 2014.
[6] B. B. Johnson, S. V. Dhople, J. L. Cale, A. O. Hamadeh, and P. T. Krein, "Oscillator-based inverter control for islanded three-phase microgrids," *IEEE Journal of Photovoltaics*, vol. 4, pp. 387–395, January 2014.
[7] B. B. Johnson, S. V. Dhople, A. O. Hamadeh, and P. T. Krein, "Synchronization of Parallel Single-Phase Inverters With Virtual Oscillator Control," *IEEE Transactions on Power Electronics*, vol. 29, pp. 6124–6138, November 2014.
[8] L. A. B. Tôrres, J. P. Hespanha, and J. Moehlis, "Synchronization of oscillators coupled through a network with dynamics: A constructive approach with applications to the parallel operation of voltage power supplies." Submitted to journal publication, Sep. 2013.
[9] L. A. B. Tôrres, J. P. Hespanha, and J. Moehlis, "Power supplies dynamical synchronization without communication," in *Proc. of the Power & Energy Society 2012 General Meeting*, July 2012.
[10] H. K. Khalil, *Nonlinear Systems*. Prentice Hall, 3 ed., 2002.
[11] S. H. Strogatz, *Nonlinear Dynamics and Chaos: With Applications to Physics, Biology, Chemistry, and Engineering*. Studies in nonlinearity, Westview Press, 1 ed., Jan. 2001.
[12] S. E. Tuna, "Synchronization analysis of coupled lienard-type oscillators by averaging," *Automatica*, vol. 48, no. 8, pp. 1885–1891, 2012.
[13] R. Rand and P. Holmes, "Bifurcation of periodic motions in two weakly coupled Van der Pol oscillators," *International Journal of Non-Linear Mechanics*, vol. 15, no. 4, pp. 387–399, 1980.
[14] A. Mauroy, P. Sacré, and R. J. Sepulchre, "Kick synchronization versus diffusive synchronization," in *IEEE Conference on Decision and Control*, pp. 7171–7183, 2012.
[15] F. Wang, J. Duarte, and M. Hendrix, "Active and reactive power control schemes for distributed generation systems under voltage dips," in *IEEE Energy Conversion Congress and Exposition*, pp. 3564–3571, Sept 2009.
[16] F. Z. Peng and J.-S. Lai, "Generalized instantaneous reactive power theory for three-phase power systems," *IEEE Transactions on Instrumentation and Measurement*, vol. 45, Feb 1996.
[17] D. W. Jordan and P. Smith, *Nonlinear ordinary differential equations*. Clarendon Press Oxford, 1987.
[18] A. Fink, "Convergence and almost periodicity of solutions of forced Liénard equations," *SIAM Journal on Applied Mathematics*, vol. 26, no. 1, pp. 26–34, 1974.
[19] P. T. Krein, *Elements of Power Electronics*. New York, NY: Oxford University Press, 1998.
[20] Q.-C. Zhong and Y. Zeng, "Parallel operation of inverters with different types of output impedance," in *Annual Conference of the IEEE of Industrial Electronics Society*, pp. 1398–1403, Nov 2013.